www.czasopisma.pan.pl PAN www.journals.pan.pl

ARCHIVES of FOUNDRY ENGINEERING

ISSN (2299-2944)
Volume 2025
Issue 1/2025

75 – 84

9/1

10.24425/afe.2025.153776

Published quarterly as the organ of the Foundry Commission of the Polish Academy of Sciences

Comparative Study on the Effect of Different Gas Types in Baking Regenerative Ladle

Jiayang He [a], Guangqiang Liu [a, *], Yuanxin Liu [a], Zhizhong Cao [b], Jun Liu [b]
[a] School of Civil Engineering, University of Science and Technology Liaoning, China
[b] Technology Research Center of Bengang, Bengang Group, China
* Corresponding author: E-mail address: lgqiang0305@sina.com

Received 28.06.2024; accepted in revised form 29.11.2024; available online 17.03.2025

Abstract

Regenerative high-temperature air combustion (HTAC) is currently the most effective technology for ladle preheating and baking. However, the impact of different gas types on regenerative ladle baking varies significantly. Thus, a comparative analysis of the effects of various gas types on ladle baking is essential for optimizing the HTAC process and identifying suitable gas alternatives for practical applications. This study specifically examines the baking of a 130 t ladle utilizing HTAC technology, with natural gas, coke-oven gas, and converter gas as fuel sources. The research compares the influence of these gas types on flame characteristics and temperature, focusing on their effects on the internal temperature and flow field within the ladle. The results indicate that natural gas, coke-oven gas, and converter gas produce flame lengths of 2.3 m, 2.6 m, and 2.83 m, respectively, after achieving stable combustion. Both natural gas and coke-oven gas demonstrate superior flame shapes and greater stability, resulting in faster ladle baking rates. The inner wall and bottom of the ladle can be heated to temperatures exceeding 1200 K using natural gas or coke-oven gas, whereas converter gas stabilizes at around 1100 K. Furthermore, the thermal efficiencies of the baking process are measured at 25.43%, 22.08%, and 7.97% for natural gas, coke-oven gas, and converter gas, respectively. Therefore, natural gas and coke-oven gas are viable alternatives to converter gas for heating steel ladles, effectively meeting the demands of industrial production.

Keyword: Ladle baking, Regenerative combustion, Gas type, Baking efficiency

1. Introduction

The preheating and baking of the ladle can increase the average temperature of the ladle working lining by 72.5-130.3K [1], which effectively preserves heat for the inner lining of the ladle. Heat storage high-temperature air combustion technology (HTAC) is currently considered as the most effective technology for ladle preheating and baking, representing a revolutionary new combustion technology. This technology involves preheating the combustion air from room temperature to 800 °C through efficient heat storage materials. The high-temperature air combustion (HTAC) technology is also referred to as excess enthalpy combustion (EEC), flameless oxidation (FLOX), or moderate and intense low oxygen dilution (MILD) combustion. The operational principle of HTAC is described as "super enthalpy combustion." In comparison with traditional combustion technology, HTAC has higher combustion efficiency, lower emissions of NOx, CO_2, and other pollutants, shorter baking time, and more uniform combustion temperature in the ladle. Currently, there are numerous studies on applying HTAC technology in ladle baking, and these findings have significantly promoted its mature application in steelmaking processes.

The use of natural gas as a heat source for HTAC has been widely established. Suzukawa et al [2] developed a low NOx burner using HTAC technology to enhance heat transfer performance and reduce NOx concentration in industrial furnaces. Yilmaz, E. [3] introduced a new type of burner based on HTAC technology with

secondary combustion of natural gas as fuel to achieve low oxygen combustion. Semagina, N. et al [4] and A et al [5] also conducted structural optimization of the burner under HTAC technology. Kawai K. et al [6] validated a new concept boiler using HTAC technology for burning natural gas, finding that preheating the air to temperatures exceeding 1273 K enhances combustion efficiency in the furnace. Jia L et al [7] conducted a study using natural gas as fuel to simulate and analyze the flame characteristics of a high temperature air combustion (HTAC) furnace. The findings indicate that the regenerative heat transfer heat recovery efficiency of high temperature air combustion is over 80%, and the temperature distribution within the furnace is nearly uniform.

In recent years, significant progress has been made in the application of artificial gas in HTAC technology. Sánchez, M. et al [8] demonstrated the advantages of oxygen enhanced flameless combustion in a self-regenerative burner using coke-oven gas as fuel. Weihong, Y. et al [9] numerically investigated the combustion performance of a semi-industrial test furnace equipped with a regenerative burner and a conventional turbulent jet burner using converter gas. The results showed that equipping the furnace with a high-cycle regenerative burner system could result in a more uniform gas temperature increase, a significant improvement in energy utilization efficiency, lower NOx emission concentration and better flame performance.

Currently, there is a lack of effective knowledge regarding the comparison of the baking effects of various gases. In practical production, the type of gas used in ladle baking is often changed due to the influence of on-site air sources. Therefore, conducting a comparative analysis of the baking effect of different types of gas on steel ladles is highly significant for optimizing the heat storage ladle baking process and determining equivalent replacements for gas in actual baking. Based on the aforementioned, this study aims to conduct research on the 130t ladle baking under HTAC technology. The study will compare the effects of using natural gas, coke-oven gas, and converter gas as fuel on flame shape and temperature, and analyze their impact on temperature and flow field in the ladle. The impact of different types of gas on ladle baking under HTAC technology is elucidated to offer a reference for industrial production.

2.Model Building

2.1 Mathematical model

This study focuses on the combustion of fuel and flow inside the ladle during the combustion process, as well as heat transfer by air convection both inside and outside the ladle. Additionally, it examines heat transfer within the ladle liner, ladle cover, and baking cover in order to establish a mathematical model of fuel combustion. The basic governing equations [10] are as follows:

Continuity equation:

$$\frac{\partial \rho}{\partial t}+\frac{\partial(\rho u)}{\partial x}+\frac{\partial(\rho v)}{\partial y}+\frac{\partial(\rho w)}{\partial z}=0 \tag{1}$$

Energy conservation equation:

$$\frac{\partial(\rho T)}{\partial t}+div(\rho u T)=div(\frac{k_t}{c_p}gradT)+S_T \tag{2}$$

Momentum conservation equation:

$$\frac{\partial(\rho u)}{\partial t}+div(\rho u u)=div(\mu gradu)-\frac{\partial p}{\partial x}+S_u \tag{3}$$

$$\frac{\partial(\rho v)}{\partial t}+div(\rho v u)=div(\mu gradv)-\frac{\partial p}{\partial y}+S_v \tag{4}$$

$$\frac{\partial(\rho w)}{\partial t}+div(\rho w u)=div(\mu gradw)-\frac{\partial p}{\partial z}+S_w \tag{5}$$

where ρ refers to the density; u, v, and w indicate the component velocity along x, y, and z directions, respectively; t refers to time; T refers to temperature; k_t refers to the thermal conductivity; c_p refers to the specific heat; S_T refers to the heat source item; u refers to the velocity vector; μ refers to dunamic viscosity; p refers to pressure.

The turbulence model uses the standard k-ε model, The transport equation consists of two parts, in which the transport equation of turbulent kinetic energy k is as follows:

$$\frac{\partial}{\partial t}(\rho k)+\frac{\partial}{\partial x_i}(\rho k u_i)=\frac{\partial}{\partial x_j}[(\mu+\frac{\mu_t}{\varphi_k})\frac{\partial k}{\partial x_j}]+G_k+G_b-\rho\varepsilon-Y_M+S_k \tag{6}$$

The turbulent dissipation rate ε can be expressed as:

$$\frac{\partial}{\partial t}(\rho \varepsilon)+\frac{\partial}{\partial x_i}(\rho \varepsilon u_i)=\frac{\partial}{\partial x_j}[(\mu+\frac{\mu_t}{\varphi_\varepsilon})\frac{\partial \varepsilon}{\partial x_j}]+C_{1\varepsilon}\frac{\varepsilon}{K}(G_k+C_{3\varepsilon}G_b)-C_{2\varepsilon}\rho\frac{\varepsilon^2}{k}+S_\varepsilon \tag{7}$$

The turbulent viscous model μ_t can be expressed as:

$$\mu_t=\rho C_\mu\frac{k^2}{\varepsilon} \tag{8}$$

where k refers to the turbulent kinetic energy; ε refers to the dissipation rate of k; G_k refers to the k generation rate generated by the average velocity gradient; G_b refers to the dissipation rate of k generated by buoyancy; Y_M refers to the contribution of pulsation expansion in compressible turbulence; S_k and S_ε are the source terms for k and ε, respectively. u_i refers to the time-average velocity; $C_{1\varepsilon}$, $C_{2\varepsilon}$, $C_{3\varepsilon}$ are empirical constants; φ_k refers to the turbulent Prandtl number of k; φ_ε refers to the turbulent Prandtl number of ε.

The radiative transfer equation (RTE) is shown in equation (9). P-1 radiation model is selected in this study, which is suitable for complex calculation with small computation amount.

$$\frac{dI(r,s)}{ds}+(a+\sigma_s)I(r,s)=aI_b(r)+\frac{\sigma_s}{4\pi}\int_0^{4\pi}I(r,s')\Phi(s,s')d\Omega' \tag{9}$$

where Φ refers to the phase function; I refers to the radiation intensity and depends on the position and direction vector; r, s, and s' reperesents the position vector, direction vector, and scattering direction vector, respectively; σ_s refers to the scattering coefficient; Ω' refers to the solid angle; a refers to the absorption coefficient.

Combustion is non-pre-gas fuel combustion, using the component PDF [11, 12] transport equation:

$$\frac{\partial}{\partial t}(\rho P)+\frac{\partial}{\partial x_i}(\rho u_i P)+\frac{\partial}{\partial \psi_n}(\rho R_n P)=-\frac{\partial}{\partial x_i}(\rho\langle u_i''|\psi\rangle P)+\frac{\partial}{\partial \psi_n}\left(\rho\left\langle\frac{1}{\rho}\frac{\partial J_{i,n}}{\partial x_i}\middle|\psi\right\rangle P\right) \tag{10}$$

where P refers to the joint probability density function of the composition; ψ refers to the space vector of the composition; $J_{i,n}$ refers to the molecular diffusion flux vector, and R_n is the reaction rate of composition n.

The density of air will change after heating, and the relationship between the concentration and density of air and ideal

gas is as follows:

$$\rho = \frac{p_{op}+p}{\frac{R}{M_W}T} \tag{11}$$

where R = 8.314 J mol-1 K^1; or the molar gas constant; p_{op} indicates the operating pressure which is taken as 101325 Pa in computation; p refers to the relative pressure which remains as a variable in the computation process; and M_W indicates the molar mass of the gas.

2.2. Physical model

1) Physical model and grid independence verification

Fig. 1. (a) depicts a schematic diagram illustrating the dimensions and monitoring points of a ladle, with a 130 t steel mill ladle as the research subject. The total height of the ladle is 3599 mm, with an inner cavity height of 3214 mm. The ladle consists of a ladle body, a pair of symmetrically aligned burners with identical dimensions, and a ladle cover. The burners include air inlets and gas inlets, with gas inlet diameters measuring 58.45 mm and 93.64 mm, and a fixed air inlet diameter of 153 mm. Flue gas generated after combustion is primarily discharged through the outlet, while a small amount may overflow from the edge of the ladle. In order to monitor temperature changes inside the ladle, five monitoring points (A, B, C, D and E) have been established. Monitoring point A is situated at the central position of the working layer at the bottom of the ladle, with a distance of 0.34 m from its base. Monitoring points B and C are located along the wall at distances of 1.39 m and 3.39 m from the bottom on the working layer. Similarly, monitoring points D and E are positioned at distances of 1.39 m and 3.39 m from the bottom on the permanent layer along the wall.

The materials utilized for constructing various parts, such as shell material for both permanent and working layers, are detailed in Table 1. It should be noted that within this context, the same material has been used for both walls and bottom part construction.

The geometric model is meshed using the ANSYS WORK Meshing software. Fig. 1. (b) depicts the schematic diagram of the ladle meshing. The overall structure is meshed with a hexahedral mesh, totaling 558,410 meshes and 602,564 nodes. The quality of the mesh is assessed by its orthogonal quality and skewness, which in turn affects the degree of discretization error. In order to optimize the mesh quality of the constructed model, a mesh independence verification is conducted by controlling the orthogonality and skewness properties of the generated mesh. Upon increasing the mesh number of the ladle from 400,000 to 550,000, it is observed that there is almost no significant change in the distributions of temperature and velocity. The variation range is found to be less than 5%. As a result, the ladle model with a grid number of 550,000 is chosen for this study.

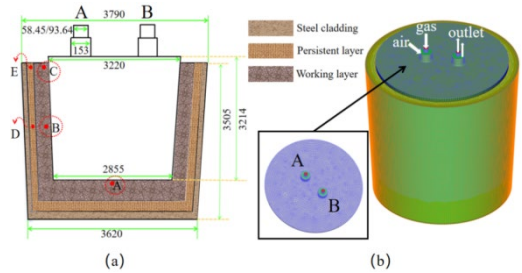

Fig. 1. Ladle size and mesh division (a) Ladle size (b) Mesh division

There are two operational modes for thermal storage ladle baking. In working mode M1, burner A serves as the inlet for air and gas, while burner B acts as the outlet for flue gas in order to store heat. Conversely, in working mode M2, the roles of burners A and B are reversed. The working cycle lasts 30 seconds, alternating between modes to maximize waste heat recovery and high-temperature preheating of combustion air. In this study, the simulated baking of empty packages was conducted online for 1.5 hours based on two modes of operation. The initial ambient temperature was set at 1069.71 K, and the preheating air temperature was maintained at 120 K. Additionally, the combustion air temperature was also set at 1200 K.

Calculate the flow rate required to bake the ladle with three different fuels, while maintaining the total heat constant. The heat released from fuel combustion is closely related to the composition of the fuel itself, and therefore, the calorific value of each fuel can be calculated using the law of mixing in the following formula.

$$H = H_1r_1 + H_2r_2 + H_3r_3 + \cdots\cdots + H_nr_n \tag{12}$$

where H refers to the high or low calorific value (kJ/Nm^3); H_1, H_2... H_n refers to the high or low calorific value (kJ/Nm^3) of each combustible component in the gas; r_1, r_2, ... r_n refers to the volumetric composition of each combustible component in a gas. The volume fractions of the three fuel components are shown in Table 2.

The calculation formula for gas heat is as follows:

$$q = HB\eta \tag{13}$$

where q refers to the heat of gas (kJ); H refers to the high or low calorific value of gas (gas mixture) (kJ/Nm^3); η refers to the Combustion efficiency (%); η in the formula is calculated according to the ideal combustion efficiency of 100 %; B refers to the gas consumption (Nm^3).

$$B = Qt_h \tag{14}$$

where Q refers to the gas flow (Nm^3/h); t_h refers to the baking time (h).

Based on the above formula, the inlet flow rates of coke-oven gas, natural gas, and coke-oven gas can be calculated as follows: Q_1 = 913.73 Nm^3/h, Q_2 = 326.17 Nm^3/h, Q_3 = 1486.75 Nm^3/h.

2) Model verification

To validate the accuracy of the numerical simulation results, an experimental platform with a similarity ratio of 1:2.5 was constructed for this study. The experimental platform consists of a steel pot with an overall height of 1439.6 millimeters, an inner

cavity height of 1285.6 millimeters, and an upper diameter measuring 1288 millimeters. The inner wall is constructed from the same three layers of material utilized in the numerical simulation, with thicknesses determined according to the aforementioned similarity ratio. Natural gas was utilized as the primary fuel, while pure oxygen served as the combustion aid. Additionally, five monitoring points were adjusted to align with those in the numerical simulation and connected to thermocouple sensors, as illustrated in Fig. 2.

The steel body was preheated to 1060 K. During this process, a continuous supply of 130 Nm^3/h of natural gas and 1363 Nm^3/h of oxygen was utilized for non-premixed combustion in order to heat treat the steel body.

At the conclusion of each 30-second commutation cycle, the gas and oxygen cylinders are promptly sealed in order to swiftly connect the gas pipe to the air intake on the opposite side. After ensuring that there are no leaks in the connection, the two cylinders are reopened for combustion and baking. The baking process is then repeated for a duration of 600 seconds. The thermocouple temperature sensor monitored the temperature change at five points A, B, C, D, and E for a duration of 600 seconds. The data was recorded, and the average temperature was calculated. Subsequently, the simulation results were compared for analysis.

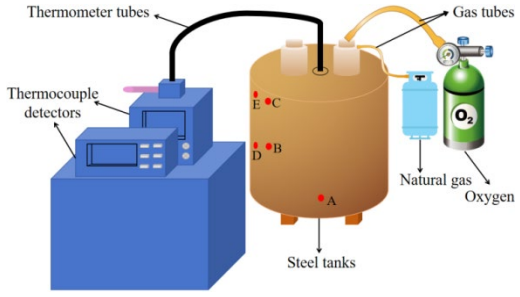

Fig. 2. Schematic diagram of the experimental platform

Fig. 3. Depicts the comparison of the final temperature between simulation and experiment after baking for 600 seconds. As depicted in the figure, the relative errors of experimental temperature and simulated temperature at points A, B, C, D, and E are 5.3%, -4.2%, -7.6%, -2.2%, and -9.8% respectively. Due to the commutation causing instability in baking temperature and the proximity of points C and E to the flame, there is a significant temperature difference between points C and E, with temperatures reaching 84.74 K and 105.22 K respectively. Point A is situated at the center of the working layer at the bottom of the ladle, thus making it highly susceptible to temperature fluctuations caused by the flame. In the actual baking process, different simulated processes exhibit stability. As a result, the experimental temperature at point A is higher than the simulated temperature, while the simulated temperature values at the other four points are higher than their respective experimental temperature values. Given the likelihood of temperature measurement errors by thermocouples under high temperature conditions, a comprehensive analysis of these errors falls within an acceptable range. This demonstrates the feasibility of the model and establishes a foundation for subsequent simulation research.

Table 1.
Thickness and material parameters of ladle wall and bottom

Hierarchy	Materials	Cladding thickness mm	Bottom thickness mm	Density kg/m^3	Specific Heat Capacity J/kg	Thermal conductivity $W \cdot m^{-1} \cdot K^{-1}$
Working layer	Magnesia-carbon brick	135	180	2900	750	2.1
Permanent layer	High alumina brick	85	130	2380	857	1.22
Ladle shell	SM490B	36	75	7830	480	56

Table 2.
Fuel component volume fraction (%)

Type/Composition	CO	CO_2	H_2	N_2	O_2	H_2O	CH_4
Natural gas	0.3	1	0.7	4	0.2	-	93.8
Coke-oven gas	9	2.3	53.6	16.4	3	-	15.7
Converter gas	60.2	14.6	1	18	0.2	5.7	-

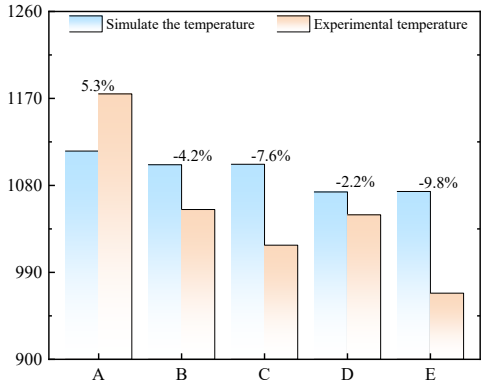

Fig. 3. Comparison of experimental temperature and simulated temperature

3. Results and analysis

3.1. Study on the influence of different gas types on flame morphology

The flame pattern significantly impacts the performance of the furnace, leading to increased maintenance and repair work. Additionally, instability in flame temperature can also affect the gas temperature. Fig. 4. illustrates the flame patterns of different radial sections for the three types of gases at various baking times. It is evident that the formation of high-temperature combustion zones varies according to the type of gas being used. Throughout the entire baking stage, natural gas and coke-oven gas maintain a consistent flame shape, whereas the flame shape of converter gas is irregular.

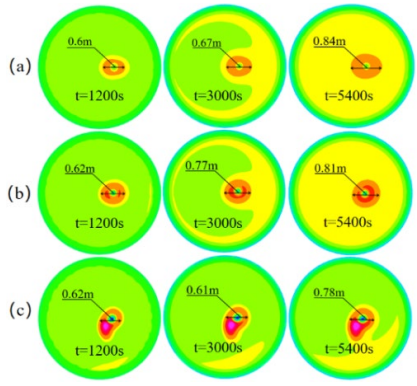

Fig. 4. Flame width of the same section in three stages (a) Natural gas (b) Coke-oven gas (c) Converter gas

During the ladle baking process, it is important to ensure that the flame length is not too long. This is to prevent the bottom temperature of the ladle from becoming excessively high, which could result in damage to the internal materials of the ladle. However, it is also crucial that the flame length is not too short, as this would not provide sufficient heat for effective baking. Characteristics such as the shape and length of a flame are influenced by the type of fuel and its flow [13] In this study, the length of the flame is defined as the distance from the burner to the center of the flame. Fig. 5. shows the axial diagram of the flame of the three fuels at the central axial section engraved at the same time. It can be seen from the diagram that the flame lengths of natural gas, coke-oven gas and converter gas are 2.3 m, 2.6 m and 2.83 m respectively. The flame length of converter gas is 8.85% longer than that of natural gas and 23.04% longer than that of coke-oven gas, respectively. When the converter gas is too long and close to the bottom of the package, a bifurcation phenomenon occurs, resulting in a soft flame that does not gather fire. This is primarily due to the complex composition of the converter gas, leading to unstable combustion performance and poor flame rigidity.

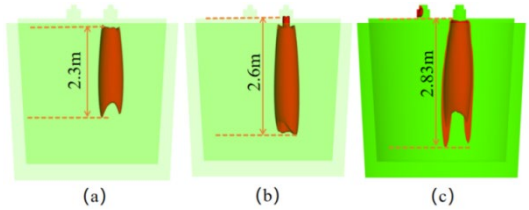

Fig. 5. Three gas flame lengths at a certain baking time (a) Natural gas (b) Coke-oven gas (c) Converter gas

3.2. Study on the influence of different gas types on flame temperature

To investigate the impact of different gas types on combustion flame characteristics, Fig. 6. illustrates the cloud map of flame temperatures for three gas types at the conclusion of baking, as well as the peak temperature within the same section. As depicted in the figure, at a height of Y=1.2 m, vortices form on both sides of the combustion area. The vortex formed near the bottom of the ladle entrains the high-temperature flue gas to the wall of the ladle, creating a vortex with low temperature inside and high temperature outside. At a height of 2.2 m, the temperature gradually increases as it approaches the flame area, reaching its peak at the center of the flame. When Y=3.2 m, the temperature near the wall approaches infinitely close to that of the flue gas at the exit. When the flue gas flows from the bottom to the top of the baking zone, the temperature is lower compared to the two preceding sections. The temperature distribution of natural gas and coke-oven gas flames is more uniform and clearly defined, while the flame temperature distribution of converter gas is irregular. This difference in flame characteristics indicates a distinct level of consistency in the combustion process for each type of gas.

The location of flame formation and the peak temperature of the flame are closer to the ladle burner [14]. This proximity allows for a longer retention time of combustion products in the combustion chamber, thereby improving the heat transfer rate of the flame. The fuel-air mixture is radially distributed, allowing for quick contact and ignition of the air and gas near the entrance where the concentration of the mixture is highest. This is the reason for the higher flame temperature. In the central section, the flame burns completely and reaches its peak. As the mixture concentration decreases along the longitudinal axis, the flame temperature also decreases and becomes uniformly distributed in the ladle. The

flame temperature of converter gas is higher than that of natural gas and coke-oven gas. Although the calorific value of natural gas and coke-oven gas is much higher than that of converter gas, it does not necessarily imply a higher flame temperature compared to that of converter gas. This is due to the fact that the proportion of alkane in natural gas and converter gas is lower than that in converter gas.

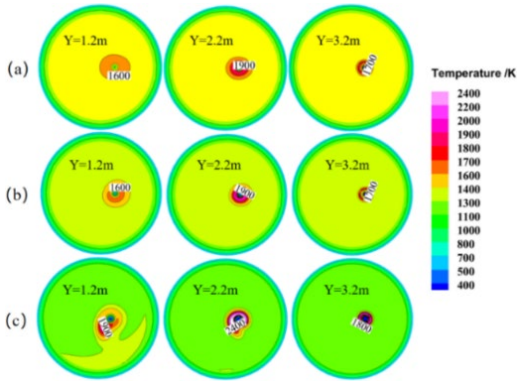

Fig. 6. Cloud image of flame temperature at the end of baking and peak temperature of section (a) Natural gas (b) Coke-oven gas (c) Converter gas

3.3. Comparative analysis of flow field inside ladle

Fig. 7. depicts the internal flow field vector diagram of three types of gas at the Z=0 section. It is evident from the diagram that the velocity distribution of each gas and air inlet aligns with the simulated setting conditions. The velocity at the inlet is high, while the velocity near the bottom of the ladle is decreasing. The velocity distribution graphs of the three types of gas exhibit noticeable differences. The velocity vector graphs of natural gas and converter gas are similar, with the high-speed zone of natural gas being wider and longer than that of converter gas. The velocity vector diagram of coke-oven gas differs from the first two types of gas, with the high-speed zone being concentrated in the center of the flame.

The velocity vector diagram is capable of reflecting only the transient changes of particles in the flow field [15]. In order to visually observe the steady state of the recirculation zone in the combustion area, a motion pattern is utilized for further analysis. When combined with the streamline distribution shown in Fig 8, it becomes apparent that air flow from the inlet nozzle is injected into the interior, collides with it at the bottom, and then spreads out around. Due to the obstructive effect of the inner wall of the ladle, smoke flows upward. The entire ladle baking area forms two asymmetrical vortices on either side of the flame, with each vortex taking on a different shape due to the varying types of gas. Air and gas are introduced into the internal baking area through the burner, where they quickly ignite in the combustion channel to create a high-speed airflow. This airflow travels in the direction of the air and gas injection, collides with the bottom of the ladle, and then flows upward along the inner wall of the ladle. Finally, the flue gas exits in a ring flow pattern at both the nozzle outlet and along the edge of the ladle. The airflow velocity within the entire combustion area is significant, resulting in the generation of negative pressure. The airflow along the inner wall of the ladle migrates towards the flame area and ultimately forms a vortex. Because of the varying speeds of air and gas injection, the resulting negative pressure also varies. As a result, the size and strength of the generated vortex differ accordingly. The vortex formed by natural gas on the left side of the combustion zone exhibits higher density but smaller width compared to the other two types of gas. In contrast, a void vortex phenomenon occurs in the right vortex of the flame burning zone for coke-oven gas, with a larger vortex density near the void vortex. With the increase in swirl number, the vortex of coke-oven gas moves closer to the combustion inlet, specifically the nozzle, and the density decreases with distance. On the right side of the combustion zone for natural gas and converter gas, a vortex is formed with a thin middle and dense outside.

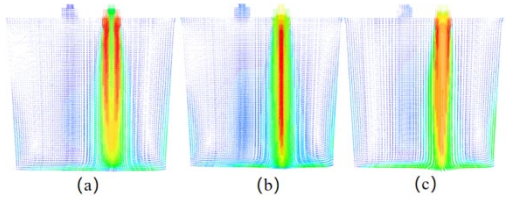

Fig. 7. Vector diagram of flow field inside ladle (a) Natural gas (b) Coke-oven gas (c) Converter gas

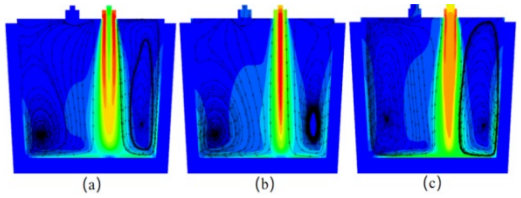

Fig. 8. Flow diagram inside ladle (a) Natural gas (b) Coke-oven gas (c) Converter gas

Fig. 9. depicts the transverse velocity distribution diagram of three types of gas on the X-axis. It is evident from the figure that as the flame center approaches, the velocity increases. Furthermore, the velocity distribution trend of all three types of gas appears to be similar. The speed distribution trend of converter gas and the other two fuels exhibits slight variations, with the peak speed occurring near X=0.25-0.30 m. Specifically, the peak speed of coke-oven gas is observed near X=0.50 m, while the peak speed of natural gas occurs near X=0.60-0.70 m.

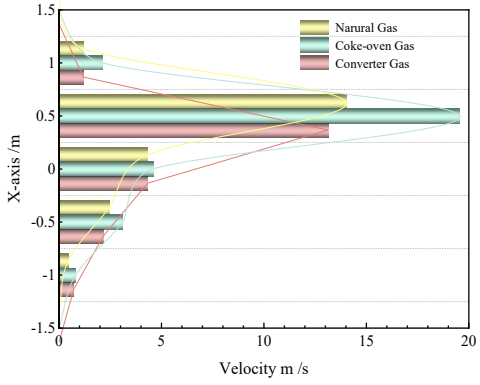

Fig. 9. X axial velocity

3.4. Comparative analysis of temperature distribution inside ladle

Fig. 10. depicts a temperature cloud map showing three different types of gas at various stages. It is evident from the map that the internal temperature of the ladle gradually increases with longer baking times. During the initial stage of baking, the flame diffusion is incomplete, resulting in non-uniform temperature distribution throughout the ladle. The high temperature area is primarily concentrated at the bottom of the ladle and near the burning flame. During the middle stage of baking, the high temperature area gradually expanded. The temperature near the inner wall of the flame side increased compared to the initial stage of baking, and there was a gradual increase in temperature at the bottom of the ladle. In the final stage of baking, the flame is fully ignited and the interior of the ladle is thoroughly heated. Due to the formation of vortices on both sides of the flame in the combustion process, a flow field is created. As a result, the high temperature flue gas generated flows upward after continuous collision with the bottom of the ladle, leading to an increase in temperature at the bottom of the ladle. In the initial stage, the high-temperature flue gas continuously loses heat in the eddy current, so the temperature inside the ladle rises slowly. With the increase in baking time, the temperature of the entire ladle baking area also rises. The influence of the vortex on temperature distribution decreases as well, eventually reaching the ideal state in the final stage.

As depicted in Fig. 10. (a), (b), the entire baking area inside the ladle reaches the on-site process temperature of 1400 K at t=5400 s when natural gas and coke-oven gas are utilized as heat sources. As depicted in Fig. 10. (c), during the initial and intermediate stages of the baking process, the high-temperature zone of the converter gas is primarily concentrated at the bottom of the ladle, with temperatures lower than those of the first two types of gas. During the middle stage of baking, the temperature throughout the furnace experiences less fluctuation compared to the early stage. At the final stage of the baking process, the temperature within the entire furnace reaches approximately 1200 K. Compared to the three types of gas, the converter gas exhibits the highest flame temperature. However, the high-temperature flue gas from the converter gas is not affected by eddy currents on both sides of the flame. As a result, a high-temperature area consistently accumulates at the bottom of the ladle, leading to non-uniform temperature distribution within the furnace. Additionally, some of the high-temperature flue gas remains at the outlet. Therefore, despite the higher combustion flame temperature of the converter gas compared to the other two kinds of gas, it has minimal impact on the temperature field in the packet.

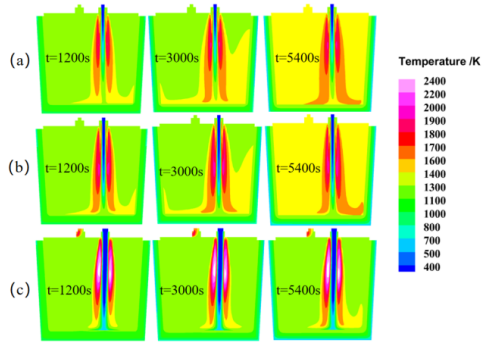

Fig. 10. Comparison of temperature cloud maps at different baking stages (a) Natural gas (b) Coke-oven gas (c) Converter gas

3.5. Comparative analysis of temperature distribution of ladle wall and ladle bottom

The effectiveness of controlling the temperature of molten steel during its subsequent transportation is directly determined by the quality of ladle lining [16]. When the refractory lining is exposed to periodic high-temperature flame baking, erosion and corrosion from molten steel can lead to structural damage, ultimately impacting the overall production operation [17-18]. As a result, the ladle lining plays a crucial role in the entire baking process. Fig. 11. illustrates the temperature cloud maps of the ladle wall and ladle bottom for three types of gas at three different stages. It is evident from the figure that the temperature of both the ladle wall and ladle bottom gradually increases during the baking process. In this study, the process of online ladle baking is simulated with an initial temperature set at 1069.71 K. Due to the thickness of the bottom and wall of the cladding, the flame has minimal impact on the heating effect of the outermost cladding. As a result, the overall temperature of the shell tends to decrease. At the conclusion of the baking process, the working layer temperature of the wall and bottom of the ladle using natural gas and converter gas can exceed 1200 K, whereas the working layer temperature when using converter gas alone reaches only about 1100 K. This is attributed to the inadequate flame shape and rigidity of the converter gas obtained above, leading to a lower final temperature at the bottom and wall of the envelope compared to the other two gases.

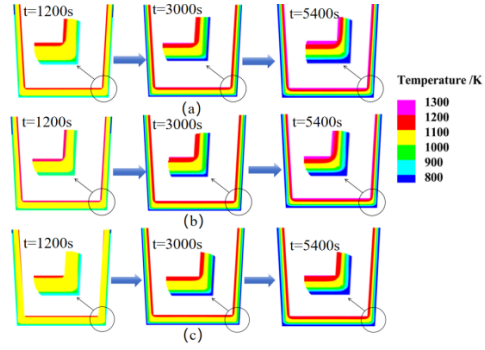

Fig. 11. Temperature field of ladle wall and ladle bottom in three stages (a) Natural gas (b) Coke-oven gas (c) Converter gas

The monitoring point A is situated at the center of the working layer at the bottom of the ladle, where temperature plays a crucial role in ensuring the safety of the entire process. And due to the greater thickness of the bottom compared to that of the wall, there is also a larger temperature difference between the interior and exterior. Fig 12 illustrates the temperature changes of three types of gas at monitoring point A over the course of baking time. It is evident from the figure that the temperature of the inner wall of the ladle continues to increase with time. Due to direct exposure to the flame, the temperature at the bottom of the cladding is higher than that at the wall. Additionally, the innermost working layer at the bottom of the cladding experiences the highest temperature [19]. In this study, the initial temperature was set at 1069.71 K. After being baked for 1.5 hours, the final baking temperatures of natural gas and coke-oven gas reached 1277.59 K and 1262.68 K, respectively, while the final temperature of converter gas as fuel was only 1207.16 K. The heating efficiency of the three types of gas at the bottom of the ladle is 0.037, 0.034, and 0.025, respectively. Additionally, the heating efficiency of converter gas is 32.43% and 26.47% lower than that of natural gas and coke-oven gas, respectively.

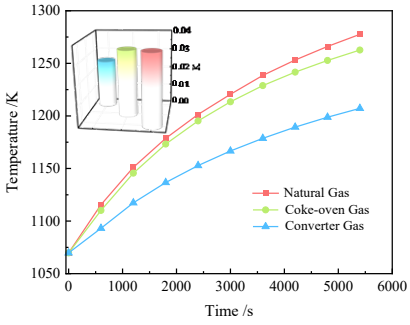

Fig. 12. Baking temperature curve of monitoring point A

Compared to the bottom of the ladle, the temperature of the ladle wall is lower. This is because the temperature of the ladle wall primarily derives from the heat brought by the flame and residual heat formed by the vortex on both sides of the flame, which in turn transfers heat to the bottom of the ladle. Fig. 13. (a) and (b) show the temperature change curves of monitoring points B and C on the working layer. It can be seen from the figure that the temperature of the working layer is higher than that of the permanent layer. This is due to the fact that the working layer is in direct contact with the furnace, and experiences direct exposure to heat and radiation. Unlike the permanent layer and ladle shell, it is influenced by material thickness. At point B, the use of natural gas as fuel results in a final temperature of 1254.89 K, representing a rise of 17.31%. The final temperature for coke-oven gas is 1243.67 K, indicating an increase of 16.26%, while the converter gas yields a final temperature of 1196.41 K, reflecting a rise of 11.84%. The heating efficiency of natural gas surpasses that of the other two types of gas, making it a more suitable fuel for rapid heating applications. The temperature at monitoring point C is lower than that at monitoring point B, which aligns with the previously described reasons and adheres to the principles of heat transfer.

Fig. 13. (c) and (d) depict the temperature rise curves of the permanent layer of the ladle. As illustrated in the figures, the final temperature of natural gas as fuel at monitoring point D is 1148.71 K, while the final temperature of coke-oven gas is 1144.02 K, and the final temperature of converter gas is 1118.63 K. Under the condition where heat is considered as the quantity, with gas type and baking time being the variables, it is observed that natural gas exhibits the largest temperature rise, while converter gas shows the smallest temperature rise. This pattern also holds true for the temperature rise rate. As monitoring point E is located near the top of the baking area, the temperature is slightly lower than that at monitoring point D. However, the difference is within 5 K, and the warming trend aligns with that at point D, thus adhering to baking regulations. In Fig. 13. (a), (b), (c) and (d), the temperature rise rate of the converter gas is 38.59%, 39.02%, 30.71% and 26.79% lower than that of natural gas, respectively, and lower than coke-oven gas by 35.36%, 35.07%, 26.78% and 21.83% respectively.

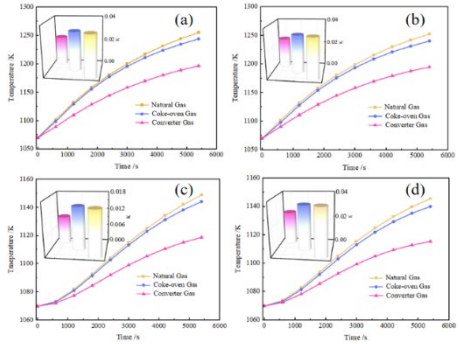

Fig. 13. Baking temperature curve of ladle wall (a) Point B (b) point C (c) point D (d) point E

Fig. 14. depicts a temperature comparison diagram at each monitoring point for three types of gas during the baking process at 3000 s and 5400 s, respectively. The diagram illustrates that when natural gas and coke-oven gas are utilized as fuel, the inner wall and bottom temperature of the ladle can ultimately stabilize above 1200 K. In contrast, when converter gas is used as fuel, the overall temperature remains around 1100 K. During the 5400-second baking process, the average temperatures of natural gas, coke-oven gas, and converter gas at the five monitoring points were recorded as 1215.77 K, 1206.06 K, and 1166.43 K, respectively. It was observed that the average temperature of converter gas was 4.06 % lower than that of natural gas and 3.29% lower than that of coke-oven gas. Upon comparison, it has been observed that the temperature of natural gas at each monitoring point exceeds that of coke-oven gas and significantly surpasses that of converter gas. In conclusion, when natural gas is utilized as the fuel for baking, it results in rapid heating of the inner wall and bottom of the ladle, leading to an effective heating effect.

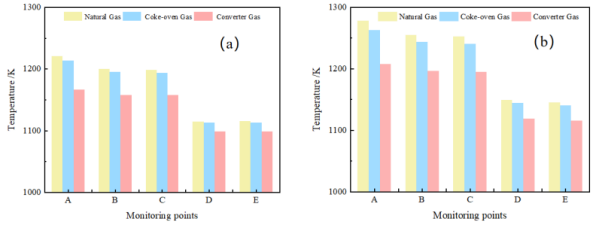

Fig. 14. Temperature at each temperature measuring point (a) 3000s (b) 5400s

3.6. Comparison of baking efficiency of different gas types

To determine the heat stored by the ladle lining and outer shell, the thermal efficiency of ladle baking is ultimately calculated. The following assumptions are made: (1) the ladle is approximately a standard cylinder with a diameter of 3790 mm and a height of 3505 mm; (2) The ladle is in a state of thermal equilibrium at every moment; (3) Contact thermal resistance between the ladle lining and the layer is disregarded. In the ladle baking process, the main heat expenditure comes from the heat storage of ladle lining and shell. The formula for bulk heat storage is as follows:

$$Q_5{}' = \frac{\Sigma m_i c_i}{\tau_1}(t_w - t_0) \tag{15}$$

where $Q_5{}'$ refers to the heat accumulation of ladle lining and outer shell (kJ /h); m_i refers to the mass of the material of each layer of ladle lining and shell (kg); c_i refers to the specific heat capacity of each layer material of ladle lining and shell [kJ /(kg·°C)]; τ_1 refers to the ladle baking time (h); t_w refers to the average temperature of inner and outer walls at the end of baking of ladle lining and shell (°C); t_0 refers to the average temperature of inner and outer walls at the beginning of baking of ladle lining and shell (°C).

The heat input of ladle baking comprises three components: fuel combustion chemical heat, fuel sensible heat, and air sensible heat. The sensible heat of the fuel is negligible, and therefore not considered in this paper. The chemical thermal calculation formula for fuel combustion is as follows:

$$\mathrm{Q_1} = \mathrm{BQ_{net,v,ar}} \tag{16}$$

Formula for calculating sensible heat of air:

$$\mathrm{Q_3} = \mathrm{B}\alpha {L_0}^S(C_k t_k - C_{kc} t_c) \tag{17}$$

where $\mathrm{Q_1}$ refers to the chemical heat of fuel combustion (kJ/ h); $\mathrm{Q_{net,v,ar}}$ refers to the low calorific value of fuel received base (kJ/m^3); $\mathrm{Q_3}$ refers to the physical quantity brought into the combustion air (kJ/h); B refers to the fuel consumption (m^3/h); α refers to the air coefficient; C_k, C_{kc} refer to the average specific heat capacity of air between 0 and t_k and t_c [kJ/(kg·°C)], respectively. ${L_0}^S$ refers to the theoretical wet air quantity (m^3/m^3).

$${L_0}^S = {L_0}^R(1 + 0.00124 g_k) \tag{18}$$

$${L_0}^R = 0.0238({H_2}^S + CO^S) + 0.0952{CH_4}^S + 0.0476(m + \frac{n}{4}){C_m H_n}^S + 0.0714{H_2S}^S - 0.0476{O_2}^S \tag{19}$$

where ${L_0}^R$ refers to the theoretical dry air quantity (m^3/m^3); g_k refers to the water content of dry air (g /m^3); Z^S refers to the volume fraction of any wet component in gaseous fuels (%).

The thermal efficiency calculation formula of regenerative ladle baking system is as follows:

$$\eta = \frac{Q_5{}'}{(Q_1 + Q_3)} * 100\% \tag{20}$$

where η refers to the efficiency of regenerative ladle baking system (%).

The thermal efficiency results for the three types of gas baking for 1.5 hours, calculated using formulas (15) to (20), are presented in Table 3. As depicted in the table, the average thermal efficiency of natural gas and coke-oven gas is 25.43% and 22.08%, respectively. Owing to the low heating value of the converter gas, the temperature in the ladle increases at a slow rate, resulting in an average thermal efficiency of only 7.97%.

Table 3.
Calculation results of baking thermal efficiency

Gas type	Q_1 (kJ /h)	Q_3 (kJ /h)	Q_5 (kJ /h)	η (%)
Natural gas	5.17×10^6	6.13×10^3	1.32×10^6	25.43
Coke-oven gas	5.17×10^6	5.45×10^3	1.14×10^6	22.08
Converter gas	5.17×10^6	4.52×10^3	4.13×10^5	7.97

4. Conclusions

In this study, the baking effects of three different fuels were compared under identical heating quantities and baking times. The results were found:

1. After achieving stable combustion, the flame lengths for natural gas, coke-oven gas, and converter gas are 2.3 m, 2.6 m, and 2.83 m, respectively. Among these, the flame shape of natural gas and coke-oven gas is superior, exhibiting greater rigidity, while the flame shape of converter gas is irregular and excessively long.
2. All three types of gas produce vortices on both sides of the flame. The heat in the high-temperature zone at the bottom of the ladle is transferred to the ladle wall through a rolling action, effectively heating it. Among them, the organization of natural gas flow is more regular.
3. Natural gas and coke-oven gas have a faster baking speed, and both are capable of heating the inner wall and bottom temperature of the ladle to over 1200 K. When baking for 5400 seconds, the average temperatures of natural gas, coke-oven gas, and converter gas at 5 monitoring points were recorded as 1215.77 K, 1206.06 K, and 1166.43 K, respectively. It was observed that the average temperature of converter gas is 4.06% lower than that of natural gas and 3.29% lower than that of coke-oven gas.
4. Given the same total heating capacity, the thermal efficiency of natural gas, coke-oven gas, and converter gas is 25.43%, 22.08%, and 7.97% respectively after a 1.5-hour regenerative baking process.
5. During the baking of regenerative ladle, natural gas and coke-oven gas may serve as alternatives to converter gas. However, their effectiveness and efficiency are contingent upon specific heating processes, equipment compatibility, as well as economic and environmental considerations. It is advisable to conduct systematic evaluations and trials throughout the substitution process to ensure both production efficiency and product quality.

Acknowledgments

The authors are grateful for the financial support by National Key Research and Development Project (2021YFB3702000), Project of Liaoning Provincial Department of Education (JYTMS20230932).

References

[1] Zhang, H., Zhou, P. & Yuan, F. (2021). Effects of ladle lid or online preheating on heat preservation of ladle linings and temperature drop of molten steel. *Energy*. 214, 118896, 1-11. https://www.sciencedirect.com/science/article/pii/S03605442 2032003X.

[2] Suzukawa, Y., Sugiyama, S., Hino, Y., Isioka, M. & Mori, I. (1997). Heat transfer improvement and NOx reduction by highly preheated air combustion. *Energy Conversion and Management*. 38(10-13), 1061-1071. https://doi.org/10.1016/S0196-8904(96)00136-7.

[3] Yilmaz, E., Ichiyanagi, M., Zheng, Q., Guo, B., Aratake, N., Kodaka, M., Hikaru, S., Okada, T. & Suzuki, T. (2023). Investigation of intake air temperature effect on co-combustion characteristics of nh3/gasoline in naturally aspirated high compression ratio engine with sub-chamber. *Scientific Reports*. 13(1), 11649, 1-12. https://link.springer.com/article/10.1038/s41598-023-38883-3.

[4] Semagina, N., Tam, R. & Sawada, J. (2022). Kinetics of low-temperature catalytic combustion of ethylene at wet conditions for postharvest storage applications. *AIChE Journal*. 68(8), e17718, 1-9. https://doi.org/10.1002/aic.17718.

[5] Weber, R., Gupta, A.K. & Mochida, S. (2020). High temperature air combustion (HiTAC): How it all started for applications in industrial furnaces and future prospects. *Applied Energy*. 278, 115551, 1-28. https://www.sciencedirect.com/science/article/pii/S03062619 20310631.

[6] Kawai, K., Yoshikawa, K., Kobayashi, H., Tsai, J.S., Matsuo, M. & Katsushima, H. (2002). High temperature air combustion boiler for low BTU gas. *Energy Conversion and Management*. 43(9-12), 1563-1570. https://doi.org/10.1016/S0196-8904(02)00036-5.

[7] Jia, L. & Li, J. (2004). The experimental study on regenerative heat transfer in high temperature air combustion. *Journal of Thermal Science*. 13, 366-370. https://doi.org/10.1007/s11630-004-0056-x.

[8] Sánchez, M., Cadavid, F. & Amell, A. (2013). Experimental evaluation of a 20 kW oxygen enhanced self-regenerative burner operated in flameless combustion mode. *Applied Energy.* 111, 240-246. https://www.sciencedirect.com/science/article/pii/S03062619 1300398X.

[9] Weihong, Y. & Blasiak, W. (2004). Combustion performance and numerical simulation of a high-temperature air–LPG flame on a regenerative burner. *Scandinavian Journal of Metallurgy*. 33(2), 113-120. https://doi.org/10.1111/j.1600-0692.2004.00675.x.

[10] Khoshhal, A., Rahimi, M. & Alsairafi, A.A. (2011). Diluted air combustion and NOx emission in a HiTAC furnace. *Numerical Heat Transfer, Part A: Applications*. 59(8), 633-651. https://doi.org/10.1080/10407782.2011.561117.

[11] Haworth, D.C. (2010). Progress in probability density function methods for turbulent reacting flows. *Progress in Energy and Combustion Science*. 36(2), 168-259. https://doi.org/10.1016/j.pecs.2009.09.003.

[12] Ma, L., Naud, B. & Roekaerts, D. (2016). Transported PDF modeling of ethanol spray in hot-diluted coflow flame. *Flow, Turbulence and Combustion*. 96, 469-502. https://doi.org/10.1007/s10494-015-9623-3.

[13] Fanjie, Y., Hui, Z., Haibin X., Azhar, M.U., Yong, Z. & Fudong, C. (2022). Numerical simulation method for the process of rockburst. *Engineering Geology*. 306, 106760. https://doi.org/10.1016/j.enggeo.2022.106760.

[14] Hosseini, A.A., Ghodrat, M., Moghiman, M. & Pourhoseini, S.H. (2020). Numerical study of inlet air swirl intensity effect of a Methane-Air Diffusion Flame on its combustion characteristics. *Case Studies in Thermal Engineering*. 18, 100610, 1-10. https://doi.org/10.1016/j.csite.2020.100610.

[15] Zhang, R.C., Bai, N.J., Fan, W.J., Yan, W.H., Hao, F. & Yin, C.M. (2018). Flow field and combustion characteristics of integrated combustion mode using cavity with low flow resistance for gas turbine engines. *Energy*. 165, 979-996. https://doi.org/10.1016/j.energy.2018.09.121.

[16] Hou, A., Jin, S., Harmuth, H. & Gruber, D. (2018). A method for steel ladle lining optimization applying thermomechanical modeling and Taguchi approaches. *JOM*. 70, 2449-2456. https://link.springer.com/article/10.1007/s11837-018-3063-1.

[17] Shuai W., Zhi, W., Dou, R., Yongli, X., Yunze, G. & Liu, X. (2022). Numerical Study on the Mixing Process of Hot Desulfurization Slag and Converter Steel Slag. *Case Studies in Thermal Engineering*. 40, 102561, 1-13. https://doi.org/10.1016/j.csite.2022.102561.

[18] Dai, Y., Li, J., Yan, W. & Shi, C. (2020). Corrosion mechanism and protection of BOF refractory for high silicon hot metal steelmaking process. *Journal of Materials Research and Technology*. 9(3), 4292-4308. https://doi.org/10.1016/j.jmrt.2020.02.055.

[19] Fang, L., Su, F., Kang, Z. & Zhu, H. (2023). Numerical simulation on heat transfer of multi-layer ladle in empty and heavy condition. *Frontiers in Heat and Mass Transfer (FHMT)*. 20, 14, 1-9. DOI: 10.5098/hmt.20.14.